scientific reports

Check for updates

OPEN

Symbiotic state affects microbiome recovery in a facultatively symbiotic cnidarian

Maria Valadez-Ingersoll, Caoimhe A. Bodnar, Emily X. Feng, Audrey Wong, Thomas D. Gilmore & Sarah W. Davies✉

Cnidarian holobionts consist of host cells, algal symbionts, and a complex microbiome residing in and on host tissue and algal symbionts. To investigate interactions among these three partners, we used antibiotics to deplete the microbiome of the facultatively symbiotic sea anemone *Exaiptasia pallida* (Aiptasia) in both symbiotic and aposymbiotic states and profiled 16S bacterial communities throughout recovery. We assessed host molecular response to microbiome depletion and recovery using RNA-seq and Western blotting of immune transcription factor NF-κB. 16S results demonstrate that, following depletion, symbiotic Aiptasia readily reestablished bacterial communities similar to control anemones. However, aposymbiotic Aiptasia microbiomes failed to reestablish control-level microbiomes even after seven days of recovery, highlighting differences between symbiotic states. Specifically, Endozoicomonadaceae reestablished to control levels in symbiotic, but not aposymbiotic, Aiptasia, suggesting a close physical association between Endozoicomonadaceae and algal symbionts. Molecular analyses showed that, during antibiotic recovery, host immune system gene expression was downregulated, but NF-κB protein levels increased, suggesting mechanisms for microbiome reestablishment following disruption. This study demonstrates the dynamics of microbiome recovery and how microbiome community members influence host gene expression in a cnidarian, providing a foundation for future research involving pairwise interactions between microorganisms and hosts.

Keywords Microbiome, Cnidaria, Aiptasia, Gene expression, NF-κB

Many cnidarian holobionts are composed of host cells, intracellular photosynthetic algae in the Family Symbiodiniaceae, and a microbiome comprising bacteria, archaea, viruses, fungi, and protists[1]. This microbiome associates with high specificity to host microhabitats[2,3] and algal symbionts[4–7]. A role for the microbiome as a protective and adaptive system for reef-building corals in the face of environmental stress, especially pathogenic disease, has been posited by the Coral Probiotic Hypothesis[8] and is supported by studies identifying antibiotic production by coral mucus-associated bacteria[9]. The Coral Probiotic Hypothesis has been used as justification for probiotic treatment of coral with Beneficial Microorganisms for Coral (BMCs) in the laboratory and in natural habitats[10,11]. BMCs are thought to facilitate a variety of benefits to coral hosts[11], and bacteria in the genus *Endozoicomonas* have emerged as BMCs of interest, although their exact role in promoting holobiont health is not fully understood[11,12]. *Endozoicomonas* has been shown to influence sulfur cycling and dimethylsulfoniopropionate (DMSP) transformation[13], carbohydrate metabolism[14], and antimicrobial properties[15], with *Endozoicomonas* strains showing clear interactions with reef-building coral hosts and their algal symbionts[16].

Understanding the mechanisms underlying symbioses is challenging in reef-building corals given that many species exhibit obligate symbioses with their Symbiodiniaceae and the loss of algal symbionts (i.e., bleaching) leads to a stressed state in the host[17]. The *Exaiptasia pallida* (Aiptasia) model system, while taxonomically distinct from stony corals and non-calcifying in nature, has emerged as a powerful tool to explore the fundamental processes governing cnidarian symbiosis because these anemones can exist with and without their algal symbionts and can be easily reared in the lab[18]. In addition, efforts have been made to generate microbiome-free (axenic) cnidarians, including using antibiotics to develop gnotobiotic Aiptasia and coral wherein microbiomes are depleted[19–21]. The establishment of gnotobiotic cnidarians can enable investigations into the effects of specific microbiome members on host and holobiont health, host molecular regulation of the microbiome, and reestablishment of the microbiome following disruption[22].

Department of Biology, Boston University, 5 Cummington Mall, Boston, MA 02215, USA. ✉email: daviessw@bu.edu

The microbiome of cnidarian hosts has been shown to be influenced by biotic[23–25] and abiotic[26–28] factors in both corals and Aiptasia. Recent studies in several coral species have associated bacterial microbiomes with coral thermal resistance. In heat challenge experiments, researchers have documented a decrease in core microbial taxa—including *Endozoicomonas*—that are associated with healthy coral[27]. In a meta-analysis of coral microbiomes in response to environmental stressors, the relative abundance of *Endozoicomonas* consistently decreased following stress events[29]. However, the relative abundance of *Endozoicomonas* can also decrease when corals are housed and fed in aquaria[12], highlighting the complexity of these relationships. This reduction in lab-reared environments may explain why multiple studies have reported an absence of *Endozoicomonas* in the Aiptasia microbiome[20,25]. There is also variation in microbiome stability. Highly stable bacterial microbiomes have been observed in *Acropora hyacinthus*[28], *Acropora millepora*, and *Turbinaria reniformis*[30], all corals with high tolerance to thermal bleaching. However, this protective effect of highly stable microbiomes may be species-specific, given that *Acropora* species have been shown to alter their microbiomes in response to environmental change (termed "microbiome conformers") whereas *Pocillopora* species maintain more stable microbiomes under these same challenges (termed "microbiome regulators")[31].

Microbiomes can affect other factors related to holobiont health, including regeneration, disease susceptibility, and nutrient cycling. Recently, in Aiptasia and reef-building corals, the microbiome and host immune system have been implicated in regeneration and wound healing[32], wherein the immune system is induced by wounding, which presumably prevents the establishment of opportunistic/pathogenic bacteria[33]. Additionally, microbiome disturbance through factors like disease and thermal stress may allow for the establishment of opportunistic or pathogenic taxa that outcompete beneficial microbiome members[34,35]. For example, Amplicon Sequence Variants (ASVs) in the order Cytophagales increased in abundance following exposure to White Band Type I disease[35] and to the pathogen *Vibrio coralliilyticus*[34], which also led to an increase in the opportunistic Rhodobacterales. Additionally, the relative abundance of disease-associated taxa (e.g., Rhodobacterales) has been found to increase following thermal stress[36,37]. Opportunistic taxa often exhibit faster growth and higher metabolic processes, providing competitive advantages during microbiome restructuring following disturbances[38,39].

To characterize interactions between a host cnidarian, its algal symbionts, and its microbiome, we have investigated the dynamics of microbiome depletion and recovery in the facultatively symbiotic sea anemone Aiptasia. We hypothesized that microbiome communities would be differentially altered by antibiotic treatment between symbiotic states, given that symbiotic Aiptasia host algae, which are known to associate with their own unique microbiome communities[6,40,41]. Additionally, we hypothesized that the host mechanisms employed during microbiome recovery would be conserved across symbiotic states in Aiptasia, given that many immune pathways associated with recognizing self-non-self are conserved across metazoans[42,43]. Using a transient antibiotic treatment, microbiomes were depleted in symbiotic (with algal symbionts) and aposymbiotic (without algal symbionts) Aiptasia, and the dynamics of microbiome reestablishment and host molecular responses to microbiome depletion and recovery were determined. Overall, this study highlights how an integrative approach exploring all holobiont partners can uncover critical relationships in tripartite symbioses in cnidarians.

Materials and methods

Aiptasia maintenance and husbandry

Aiptasia husbandry was performed as described previously[44,45]. Briefly, adult CC7 Aiptasia in symbiosis with *Symbiodinium linucheae* were maintained in 35 ppt artificial seawater (ASW, Instant Ocean) in polycarbonate tanks at room temperature (approximately 25 °C) under a 12 h:12 h light:dark cycle (white fluorescent light, 25 µmol photons m^{-2} s^{-1}). Water changes were performed weekly unless otherwise noted. Aiptasia were fed three times per week with freshly hatched Artemia nauplii. To avoid contamination with water-born bacteria, bacteria-free artificial seawater (FSW) was generated via vacuum filtration through a 0.2 µm Nylon membrane filter and used where noted.

Generation of Aposymbiotic Aiptasia

Aposymbiotic Aiptasia were generated at least three months prior to experimentation[46]. Symbiotic Aiptasia were incubated in 0.008% menthol (from a 20% w/v menthol stock in 100% ethanol) in ASW for two weeks with daily menthol solution changes. After two weeks, aposymbiotic status was verified by lack of symbiont autofluorescence under fluorescence microscopy (Leica M165 FC), and aposymbiotic anemones were then maintained in ASW. Feeding was suspended during bleaching but was resumed following confirmation of aposymbiotic state. During and after bleaching, aposymbiotic Aiptasia were maintained in darkness until at least three days prior to antibiotic treatment, at which time aposymbiotic Aiptasia were moved to the 12 h:12 h light:dark regimen.

Generation of microbiome-depleted Aiptasia

Antibiotic solution (ABS) was prepared as described previously[20]. Stock solutions of antibiotics consisted of the following: rifampicin (50 mg/ml in DMSO), nalidixic acid (50 mg/ml in MilliQ water), carbenicillin (100 mg/ml in MilliQ water), and chloramphenicol (50 mg/ml in 100% ethanol). ABS was used at a final concentration of 50 µg/ml of each antibiotic in ASW. The final ABS was vacuum filtered through a 0.2 µm Nylon membrane filter and stored in the dark at 4 °C to be used within one month. All Aiptasia were starved for two weeks prior to treatment to clear the digestive tract of microbiota associated with Artemia. Four ABS exposure conditions for each symbiotic state were used: (1) Aiptasia treated with 0.2 µm filter-sterilized ASW (FSW) for two weeks (control, C); (2) Aiptasia treated with ABS for seven days then washed twice in FSW (R0); (3) Aiptasia treated with ABS for seven days followed by two days of recovery in FSW (R2); and (4) Aiptasia treated with ABS for seven days followed by seven days of recovery in FSW (R7). ABS and FSW were changed daily throughout the experiments.

Quantification of colony-forming units

Bacterial loads of control and antibiotic-treated Aiptasia were quantified using Colony Forming Units (CFUs) for eight individuals per symbiotic state per treatment, except for aposymbiotic R0, which used six individuals (n = 62 total anemones). Briefly, individuals were placed in 100 µl FSW in individual tubes, homogenized with a sterile pestle, and serially diluted to 1:1000 (i.e., 1:1, 1:10, 1:100, 1:1000). 1 µl of each dilution was plated on Marine Agar. Eight negative controls of 1 µl of FSW were additionally plated. Plates were incubated at 25 °C for 48–72 h, and colonies were counted to calculate total CFUs for each individual (accounting for dilution factor and total volume of lysis). To normalize for bacteria present in the FSW, CFUs counted on the negative control FSW-alone plates were averaged, and this average was multiplied by 100 to account for the total volume of FSW used in the anemone homogenization. This number was subtracted from the total CFUs calculated for each individual. CFUs across treatments within symbiotic states were compared using Kruskal–Wallis and Dunn's post-hoc tests in the FSA package v.0.10.0[47]. It should be noted that this CFU approach fails to detect bacteria that are incapable of growing on Marine Agar, so this approach could be an underestimate of total bacterial load.

Quantification of symbiosis by red channel intensity

To assess changes in pigmentation (a proxy for symbiont density) over the course of antibiotic treatment in symbiotic Aiptasia, red channel intensity was measured for fifteen individuals from each condition at the beginning and end of the experiment. Anemone photographs (taken in standardized conditions with an iPhone 15 Pro at 2 × magnification) were white-balanced in Adobe Photoshop (v.26.5.0). Images were analyzed in Matlab (v.R2025a) following the Coral Color Intensity Analysis Utility 1.0 program[48] to extract red values (R-values). Three points from anemone tentacles were randomly chosen, measured, and averaged for each image. The relative change in R-value per anemone (measured as (final-initial)/initial) was compared across treatments using an analysis of variance and Tukey's post-hoc test for pairwise comparisons[49].

Generation of 16S gene sequencing microbiome libraries

To characterize bacterial communities associated with microbiome depletion and recovery in symbiotic and aposymbiotic Aiptasia, 5–7 individuals from each treatment condition (C, R0, R2, R7) were prepared for 16S gene sequencing (n = 48). Libraries were generated using a series of PCR amplifications of the V4/V5 region of the bacterial 16S rRNA gene[50,51] as follows: 95 °C for 40 s, 58 °C for 120 s, 72 °C for 60 s for 33 cycles, with a final elongation step of 72 °C for 5 min. PCR products were purified using GeneJET PCR Purification kits (ThermoFisher), and each PCR product was barcoded via five PCR cycles and visualized on a 1% agarose gel to assess relative concentrations. Five negative controls using sterile water were prepared and used to remove contaminating sequences. Samples were pooled in equimolar concentrations, gel-extracted, and submitted for paired-end 250 bp sequencing on an Illumina Miseq at Tufts University Core Facility.

Analysis of bacterial community

All 16S analyses were performed in RStudio (v.4.4.0)[49,52] following previously published work[32,53]. 16S primers were removed from raw reads using cutadapt[54]. DADA2 v.1.24.0[55] performed quality filtering (including removing off-target length reads and chimeras), resulting in the identification of 1,419 amplicon sequence variants (ASVs). Taxonomy was assigned at 100% sequence identity using the Silva v.138.1 database[56]. 83 ASVs matching mitochondria, chloroplasts, or non-bacterial kingdoms were removed. Finally, decontam v.1.26.0[57] was used to remove 87 contaminating ASVs based on co-occurrence with negative controls. Underrepresented ASVs (ASVs in less than 0.02% of counts) were removed using MCMC.OTU v.1.0.10[58], resulting in a total of 264 ASVs across samples used in downstream analyses.

The effect of treatment on bacterial communities between symbiotic states was assessed via Principal Coordinate Analyses (PCoA), and a PERMANOVA compared Aitchison distances between samples by modeling the combined effect of treatment and symbiotic state[59,60].

Vegan v.2.7-0[60] rarefied cleaned counts to 5,617 counts per sample, which was the minimum count number observed across all samples. Alpha diversity metrics (Inverse Simpson's Index, Shannon Index, ASV Richness, and Evenness) then further assessed bacterial communities across treatments using phyloseq v.1.50.0 (function *estimate_richness*[61]). The Inverse Simpson's Index values were natural-log-normalized. The interaction between treatment and symbiotic state was measured using a two-way ANOVA for each Alpha diversity metric, and Tukey's post hoc made pairwise comparisons[49].

Rarefied data were used to determine differences in relative abundance of different taxa across treatment and symbiotic state. First, the relative abundances of all ASVs across treatment and symbiotic state were visualized in a bar plot[61] separated by Phylum and Class. Next, ASVs assigned to the Phylum Proteobacteria (the most abundant Phylum in all samples) were identified, and Proteobacteria relative abundances across treatment and symbiotic state—separated by Family—were visualized in a bar plot[61]. Finally, relative abundance counts from all ASVs in the Family Endozoicomonadaceae were compared across treatment conditions and symbiotic states. Summary statistics were computed[62] for each condition and compared using a two-way ANOVA and Tukey's post-hoc test[49].

DESeq2 v.1.44.0[63] was used to determine differentially abundant ASV counts of all ASVs across treatments and symbiotic states. Pairwise comparisons were performed between each treatment relative to controls within each symbiotic state, and significant ASVs were identified with a p-adjusted value cutoff of 0.05. The $\log_2$-transformed abundance of each differentially abundant ASV in each anemone relative to the mean ASV abundance across all anemones was visualized in a heatmap[64], and Phylum was noted.

RNA extraction

To examine host gene expression, we performed TagSeq 3' RNA-based library preparation on symbiotic and aposymbiotic Aiptasia from each antibiotic treatment[45]. Four to six individuals of each treatment/symbiotic state (n = 40 total anemones) were flash frozen, and total RNA was extracted using the RNAqueous Total RNA Isolation Kit (Invitrogen) according to the manufacturer's instructions. RNA quantity and integrity were assessed using a DeNovix DS11 + Spectrophotometer. Samples were normalized to 10 ng/µl and submitted to the University of Texas at Austin Genomic Sequencing and Analysis Facility for TagSeq Library Preparation (as performed previously[65]), and these libraries were sequenced on a NextSeq 1000 P2, 300 cycle (per 10 M reads).

Analysis of RNA-sequencing data

Raw fastq reads were processed following an established pipeline (https://github.com/z0on/tag-based_RNAseq). Briefly, fastx_toolkit trimmed adapters and poly(A) + tails, PCR duplicates were removed, and short (< 20 bp) and low-quality reads (quality score of ≤ 20) were discarded[66]. Cleaned reads were mapped to concatenated *E. pallida*[67] and *S. linucheae*[68] transcriptomes using Bowtie2[69]. A raw counts file containing all genes mapping exclusively to Aiptasia was used in downstream analysis (Supplementary Dataset 1). Genes mapping to *S. linucheae* were not analyzed due to low counts.

All downstream analyses of RNA-sequencing data were performed in R v.4.4.0[49,52]. DESeq2 v.1.44.0[63] identified differentially expressed genes (DEGs) between pairwise comparisons of interest by modelling all samples by condition (combined factor of symbiotic state and antibiotic treatment). ArrayQualityMetrics (v.3.62.0)[70] tested for outliers, identifying one aposymbiotic R2 individual as an outlier, which was subsequently removed. Individual contrasts between treatments within each symbiotic state and between symbiotic states within each treatment identified DEGs (FDR-adjusted-p-value < 0.05) for 16 pairwise comparisons. Count data were *rlog*-normalized, and overall gene expression patterns were compared across all treatments through a Principal Component Analysis (PCA) implemented in vegan (v.2.7–0)[60] followed by a PERMANOVA implemented with the pairwiseAdonis package v.0.4.1[59]. Differential enrichment of gene pathways following microbiome depletion and recovery within each symbiotic state was investigated by exploring Biological Process (BP) Gene Ontology (GO) term enrichment via the Mann–Whitney U tests (GO-MWU) on all genes in each of six pairwise comparisons (*aposymbiotic-R0:aposymbiotic-C; aposymbiotic-R2:aposymbiotic-C; aposymbiotic-R7:aposymbiotic-C; symbiotic-R0:symbiotic-C; symbiotic-R2:symbiotic-C; symbiotic-R7:symbiotic-C*)[71]. Significantly enriched GO terms (FDR-p-value < 0.1) were plotted in dendrograms. Delta rank values of BP GO terms enriched in at least two of the six comparisons were visualized in ggplot2 (v.3.5.1)[72] to compare differences in enrichment across treatments and symbiotic states.

To identify clusters of genes highly correlated to host condition (symbiotic state, normalized CFU, relative abundance of total Endozoicomonadaceae ASVs, and change in R-value (in symbiotic-only WGCNA)) and treatments (C, R0, R2, R7), a weighted gene co-expression network analysis (WGCNA) was used[73]. Because normalized CFU, relative abundance of total Endozoicomonadaceae ASVs, and change in R-value data were measured from different individual anemones, these data points were averaged across treatments and applied to individuals matching their treatment. First, a WGCNA for all Aiptasia of both symbiotic states was performed using a signed network, a softPower of 7, a minimum module size of 95 genes, and a threshold of 0.25 to merge modules with similar eigengene expression. Trait data and treatments were correlated with module eigengene expression using Pearson Correlation Coefficients, and Student asymptotic p-values were calculated for each pairwise correlation. Next, WGCNAs were performed separately for symbiotic and aposymbiotic Aiptasia following the same protocol (softPower = 15, threshold = 0.45)[73,74]. The Gray module containing 12 unassigned genes was removed from the aposymbiotic-only WGCNA. For each WGCNA, pairwise correlations between traits/treatments and module eigengenes were visualized in heatmaps, and module size was visualized in bar plots (ggplot2 (v.3.5.1)[72]). BP GO term enrichment analysis was performed on the genes included in each module using Fisher's Exact Tests (gene presence/absence in the module)[71]. Significantly enriched GO terms (FDR-p-value < 0.1) were plotted in dendrograms, and modules enriched for immune terms were further explored (Tables S1, S2, and S3). In the aposymbiotic-only WGCNA, significantly enriched BP GO terms involved in immunity were identified in the Blue module (Table S2). Genes annotated with these immune GO terms were subsetted from the Blue module if they were identified as differentially expressed (FDR-p-value < 0.05 from DESeq2) in any treatment condition (R0, R2, or R7) compared to the control. In the symbiotic-only WGCNA, significantly enriched BP GO terms involved in immunity were identified in the Black module (Table S3). Genes annotated with these immune GO terms were subsetted from the Black module if they were identified as differentially expressed (FDR-p-value < 0.05 from DESeq2) in any treatment condition (R0, R2, or R7) compared to the control. Gene expression levels across samples were visualized using pheatmap v.1.0.12[64].

Western blotting of NF-κB

Western blotting of NF-κB was performed as described previously on whole anemone extracts from three Aiptasia of each treatment and symbiotic state[44,45,75]. Western blots were repeated three times with different individuals for symbiotic Aiptasia and twice with different individuals for aposymbiotic Aiptasia. For each Western blot, three anemones per treatment were used (total of 60 anemones). Briefly, individual anemones were homogenized in 60 µl of 2 × SDS-sample buffer (0.125 M Tris–HCl [pH 6.8], 4.6% w/v SDS, 20% w/v glycerol, 10% v/v β-mercaptoethanol, 0.1% w/v bromophenol blue) using a pestle followed by heating at 95 °C for 10 min. Samples were centrifuged (10 min at 13,000 rpm) and the supernatant was collected. Extracts were electrophoresed on 7.5% SDS–polyacrylamide gels, and proteins were transferred to nitrocellulose membranes. Membranes were blocked for 1 h in TBST (10 mM Tris–HCl [pH 7.4], 150 mM NaCl, 0.05% v/v Tween 20, 5% w/v non-fat powdered milk), then incubated overnight at 4 °C with primary rabbit anti-Ap-NF-κB antiserum[44] (diluted 1:5,000). Membranes were washed five times with TBST and incubated for 1 h with secondary goat-anti-

rabbit-HRP conjugated antiserum (1:4,000; Cell Signaling Technology). After further washing, immunoreactive proteins were detected with SuperSignal West Dura Extended Duration Substrate (Fisher Scientific) and were imaged on a Sapphire Biomolecular Imager. Bands corresponding to processed (~ 50 kDa) Aiptasia NF-κB (Ap-NF-κB) were normalized to total protein loaded in each lane using Ponceau S stain and ImageJ. Unprocessed NF-κB and non-specific higher molecular weight bands are visible in some of the full-length Western blots (Fig. S1); however, levels of unprocessed NF-κB and non-specific bands were not included in the area used for quantification of NF-κB levels. For each individual anemone, normalized Ap-NF-κB values were compared to the average normalized control Ap-NF-κB for each respective blot. The relative values were plotted using ggplot (v.3.5.1)[72], and the effects of antibiotic treatment and symbiotic state on relative normalized Ap-NF-κB levels were measured using an analysis of variance[49].

Results

Antibiotic treatment depletes bacterial load and alters pigmentation in Aiptasia

To measure the effect of antibiotic treatment on bacterial load, total colony forming units (CFUs) of bacteria isolated from anemones across treatments and symbiotic states were quantified. Four treatment groups were used: (1) Control Aiptasia (C) incubated in FSW for two weeks; (2) Aiptasia treated with antibiotic solution (ABS) for seven days with no recovery period (R0); (3) Aiptasia treated with ABS for seven days followed by two days of recovery in FSW (R2); and (4) Aiptasia treated with ABS for seven days followed by seven days of recovery in FSW (R7). Directly after antibiotic treatment (R0), bacterial load significantly decreased in symbiotic and aposymbiotic Aiptasia compared to control anemones (decrease of ~ 125-fold in symbiotic and ~ 1,500-fold decrease in aposymbiotic Aiptasia; FDR p-value of < 0.05). In both symbiotic states, anemones reestablished bacterial loads that were not significantly different from control anemones within two days (R2), and these levels were maintained for up to seven days after antibiotic treatment (R7) (Fig. 1a). Notably, overall bacterial load was ~ eightfold higher in aposymbiotic controls compared to symbiotic controls (FDR p-value < 0.05). Bacteria unable to grow on Marine Agar were not quantified here.

To determine the impact of antibiotic treatment on algal symbiont densities in symbiotic Aiptasia, red channel intensity (R-value, a proxy for symbiont density) of symbiotic Aiptasia was measured at the beginning and at the end of the experiment, and changes in R-values were computed. A positive change in R-value indicates a decrease in pigmentation and presumed symbiont density loss[48]. R2 anemones experienced some bleaching (mean change of 0.18 in R2 compared to −0.13 in control anemones; FDR p-value < 0.05), but anemones recovered from algal loss by R7 (the mean change of 0.026 in R7 was not significantly different from the mean change of −0.13 in control anemones) (Fig. 1b).

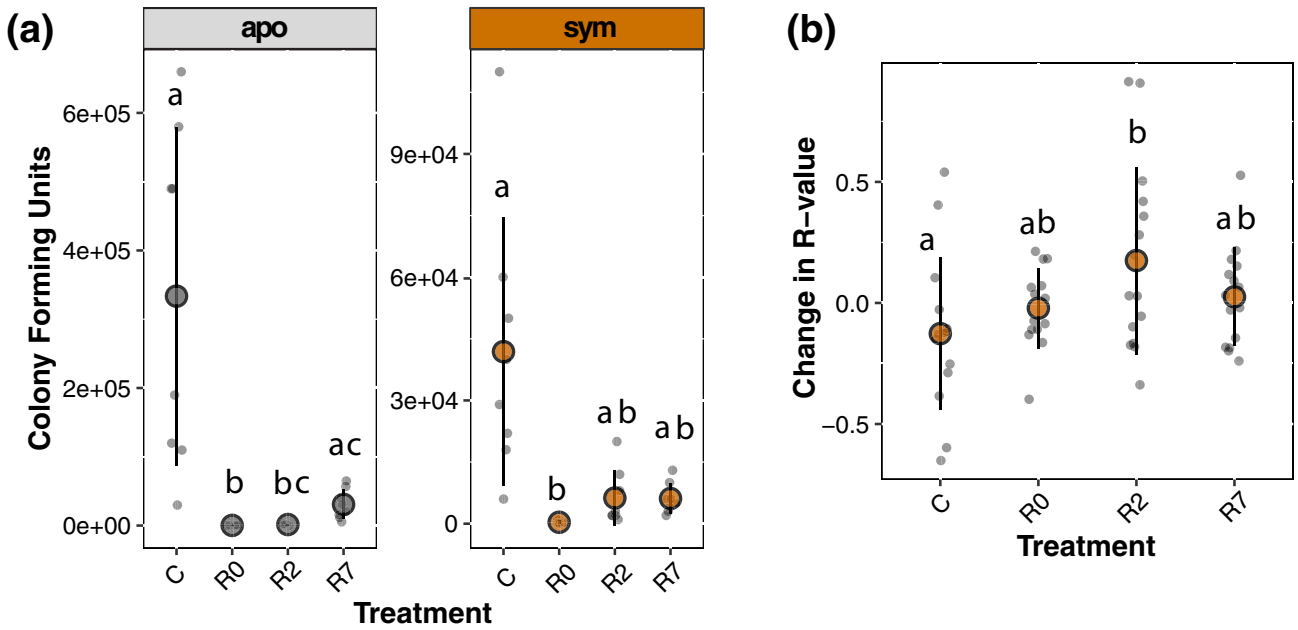

Fig. 1. Antibiotic treatment results in depletion of bacterial load in aposymbiotic and symbiotic Aiptasia and reduced pigmentation in symbiotic anemones. (**a**) Mean bacterial load estimated by total colony forming units (CFUs) from eight anemones per treatment per symbiotic state (six anemones in aposymbiotic R0). In each symbiotic state, distinct letters represent significant differences between treatments (Kruskal–Wallis and Dunn's post-hoc tests, $p < 0.05$). (**b**) Relative change in red channel intensity (R-value, proxy for pigmentation) for 15 symbiotic anemones from each treatment as measured at the beginning and end of the experiment ((final-initial)/initial). Distinct letters represent significant differences between treatments (analysis of variance and Tukey's post-hoc test, $p < 0.05$), and higher values indicate reduction in pigmentation. In (**a**) and (**b**), colored circles (gray, apo; orange, sym) show the mean, and black bars indicate standard deviation.

Microbial depletion and recovery alter alpha and beta diversity, but differ by symbiotic state

We profiled the bacterial communities of symbiotic and aposymbiotic Aiptasia from control (C), R0, R2, and R7 conditions (n = 48) (Fig. S2), resulting in 2,250,769 sequences with a mean depth of coverage of 46,891 ± 21,710 (mean ± SD) per sample (Table S4). Rarefication yielded a total of 5,617 reads per sample with a total of 264 unique ASVs identified across samples.

To investigate how antibiotic treatment alters microbiome communities following depletion and recovery, we compared 16S community composition and alpha diversity metrics for each treatment and symbiotic state. Principal Coordinate Analyses (PCoAs) revealed that overall communities differed significantly by antibiotic treatment ($p_T < 0.001$) in both aposymbiotic (Fig. 2a) and symbiotic (Fig. 2b) anemones. Within both symbiotic states, all pairwise comparisons of Aitchison distances (a beta-dispersion index of sample dissimilarity) among antibiotic treatments were significant (FDR p-value < 0.05) (Fig. 2a, b).

Alpha diversity between antibiotic treatments within each symbiotic state was measured by calculating the natural log of the Inverse Simpson's Index, the Shannon Index, Richness, and Evenness. Treatment ($p < 0.05$) and the interaction between treatment and symbiotic state ($p < 0.001$) significantly affected Simpson's Index (Fig. 2c) and Shannon Index (Fig. 2d) values. Within aposymbiotic Aiptasia, R0 anemones had higher Simpson's and Shannon Indices as compared to all other treatments ($p < 0.05$; Fig. 2c, d). Within symbiotic Aiptasia, R0 anemones had lower Simpson's and Shannon Indices than control and R7 ($p < 0.05$), but not R2 samples (Fig. 2c, d). Treatment ($p < 0.001$) and symbiotic state ($p < 0.01$), but not their interaction, had significant effects on ASV Richness (Fig. 2e). Within aposymbiotic Aiptasia, Richness was lower in R0 compared to controls ($p < 0.05$; Fig. 2e). Within symbiotic Aiptasia, Richness was lower in R0 and R2 compared to controls ($p < 0.05$; Fig. 2e). Treatment ($p < 0.01$) and the interaction between treatment and symbiotic state ($p < 0.001$) had significant effects on Evenness (Fig. 2f). Within aposymbiotic Aiptasia, Evenness was highest in R0 but returned to control levels by R2 ($p < 0.05$; Fig. 2f). Within symbiotic Aiptasia, Evenness was higher in R7 samples than in R0 samples ($p < 0.05$; Fig. 2f). Overall, alpha diversity results indicate that microbiome reestablishment dynamics following antibiotic treatment differed by symbiotic state.

Endozoicomonadaceae decrease in aposymbiotic but increase in symbiotic Aiptasia following antibiotic treatment

To investigate how specific microbial taxa were altered following antibiotic treatment and recovery, we compared the relative abundance of different taxa within each symbiotic state. Across treatments and symbiotic states, Proteobacteria was the dominant Phylum (Fig. S3a) and Gammaproteobacteria and Alphaproteobacteria were the dominant Classes (Fig. S3b). In aposymbiotic Aiptasia, the relative abundance of Endozoicomonadaceae (Phylum Proteobacteria, Class Gammaproteobacteria) decreased following antibiotic treatment (~ 38% of total ASVs in control anemones; ~ 0.03% in R0 anemones) and remained low even in R7 samples (~ 0.18% of total ASVs), suggesting a failure of this taxa to recover (Fig. 3a, b; $p < 0.001$). Interestingly, in symbiotic anemones, the relative abundance of Endozoicomonadaceae increased following antibiotic treatment at R0 and R2 (25% in control anemones; ~ 76% in R0; ~ 60% in R2) (Fig. 3a, b; $p < 0.01$). While the relative abundance of Endozoicomonadaceae was lower in symbiotic R7 anemones compared to symbiotic control anemones, this difference was not statistically significant (Fig. 3a, b).

ASV composition recovers in symbiotic but not aposymbiotic Aiptasia

To determine how individual ASVs were impacted by antibiotic treatment and recovery, we performed differential abundance analyses using DESeq2[63]. In aposymbiotic samples, there were 16 differentially abundant ASVs between R0 and control samples, 8 between R2 and control samples, and 25 between R7 and control samples (FDR p-value of < 0.05). In symbiotic samples, there were 47 differentially abundant ASVs between R0 and control samples, 40 between R2 and control samples, and 16 between R7 and control samples (FDR p-value of < 0.05), suggesting that bacterial communities return to baseline during recovery (Fig. 4). Although there were fewer overall differentially abundant ASVs in aposymbiotic than symbiotic anemones, R7 community composition in aposymbiotic anemones was more distinct from controls than R0 was from controls, indicating that microbiome communities in aposymbiotic Aiptasia failed to return to baseline as quickly as in symbiotic Aiptasia (Fig. 4).

Differentially abundant ASVs were dominated by Proteobacteria. In agreement with Fig. 3a, b, three of four Endozoicomonadaceae ASVs (ASVs 1, 3, and 7) had lower abundances in R0, R2, and R7 samples compared to aposymbiotic controls (FDR p-value < 0.05; Fig. 4). In contrast to the results from Fig. 3b, individual Endozoicomonadaceae ASVs were not significantly higher in symbiotic R0 and R2 samples compared to controls, but they were significantly lower in R7 samples (FDR p-value < 0.05; Fig. 4). Endozoicomonadaceae decreases immediately following antibiotic treatment in aposymbiotic but not symbiotic Aiptasia suggest that Endozoicomonadaceae in symbiotic anemones are buffered from antibiotic-induced loss.

Immune system pathways are downregulated during microbiome reestablishment in symbiotic and aposymbiotic Aiptasia

To determine the influence of microbiome depletion and recovery on Aiptasia gene expression, overall gene expression patterns across antibiotic treatments and symbiotic states were compared using a Principal Component Analysis (PCA). The PCA revealed a significant effect of symbiotic state on gene expression, displayed by sample separation along PC1 ($p_{Sym} < 0.001$), which explained 18.5% of the variation (Fig. 5a). Antibiotic treatment also had a significant effect on gene expression, with samples separating along PC2 ($p_T < 0.001$), which explained 7.7% of the variation (Fig. 5a). Additionally, the interaction between treatment and symbiotic state was significant ($p_{T*Sym} < 0.001$).

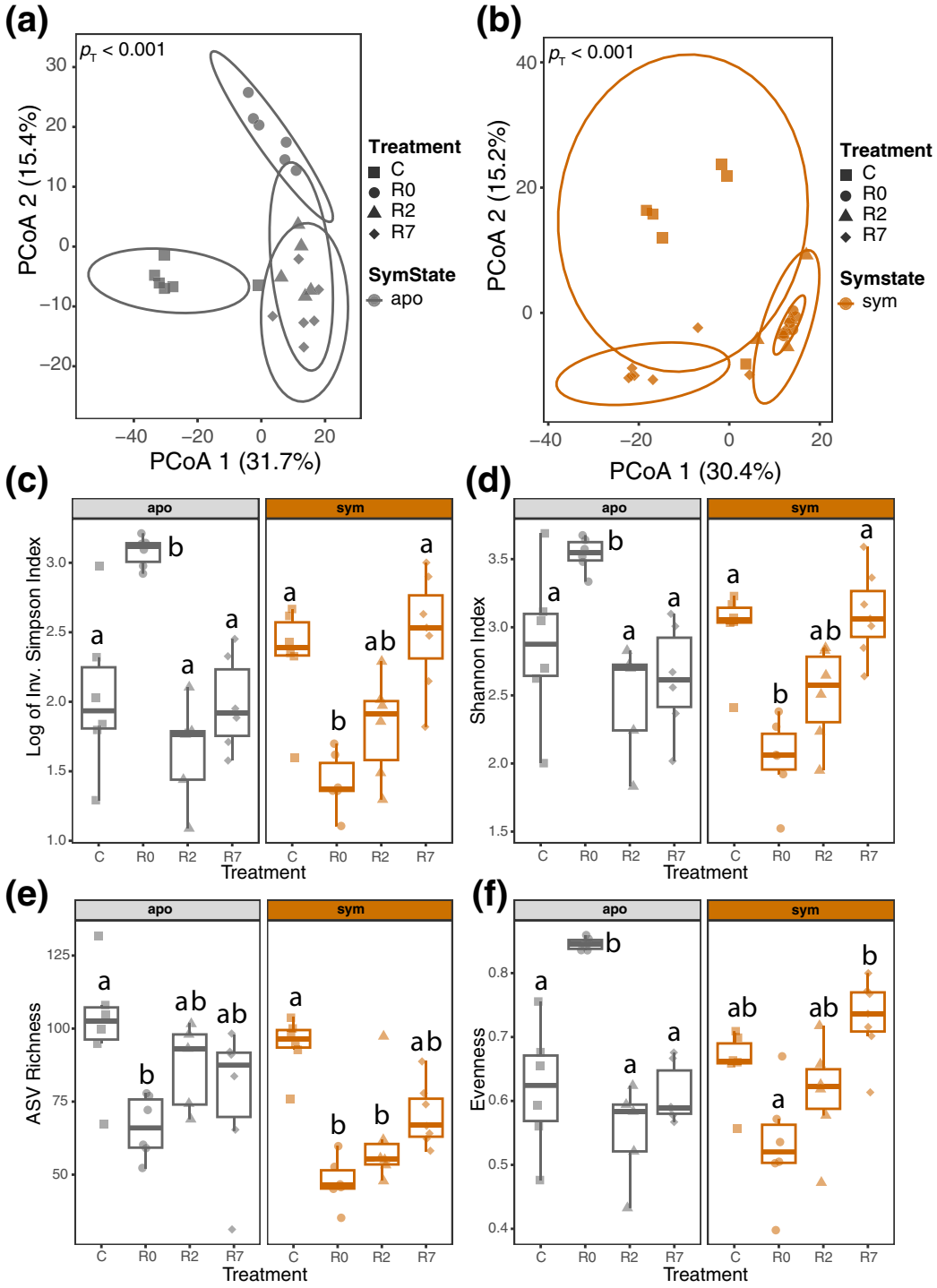

Fig. 2. Microbiome depletion and recovery alter diversity metrics in symbiotic and aposymbiotic Aiptasia. PCoAs display the similarity in bacterial communities from all ASVs in 16S data from aposymbiotic (**a**) and symbiotic (**b**) Aiptasia across antibiotic treatments (shapes). PERMANOVA results for the effect of treatment (p_T) for each symbiotic state are included in (**a**) and (**b**). Alpha diversity metrics (Natural log of the Inverse Simpson's Index (**c**); Shannon Index (**d**); Richness (**e**); and Evenness (**f**)) of rarefied 16S data were measured across symbiotic states and treatment conditions. In each symbiotic state, distinct letters represent significant differences in alpha diversity metrics between treatments (ANOVA and Tukey's post-hoc tests, $p < 0.05$). Box plots show the median and the 1st and 3rd quartiles (hinges). Whiskers extend to the maximum and minimum points if they fall within 1.5 × the Interquartile Range (if no whiskers are drawn, points outside of the box are outliers). Each point represents the alpha diversity metric of one anemone, with shapes representing antibiotic treatments and colors (gray, apo; orange, sym) representing symbiotic state, as in (**a**) and (**b**).

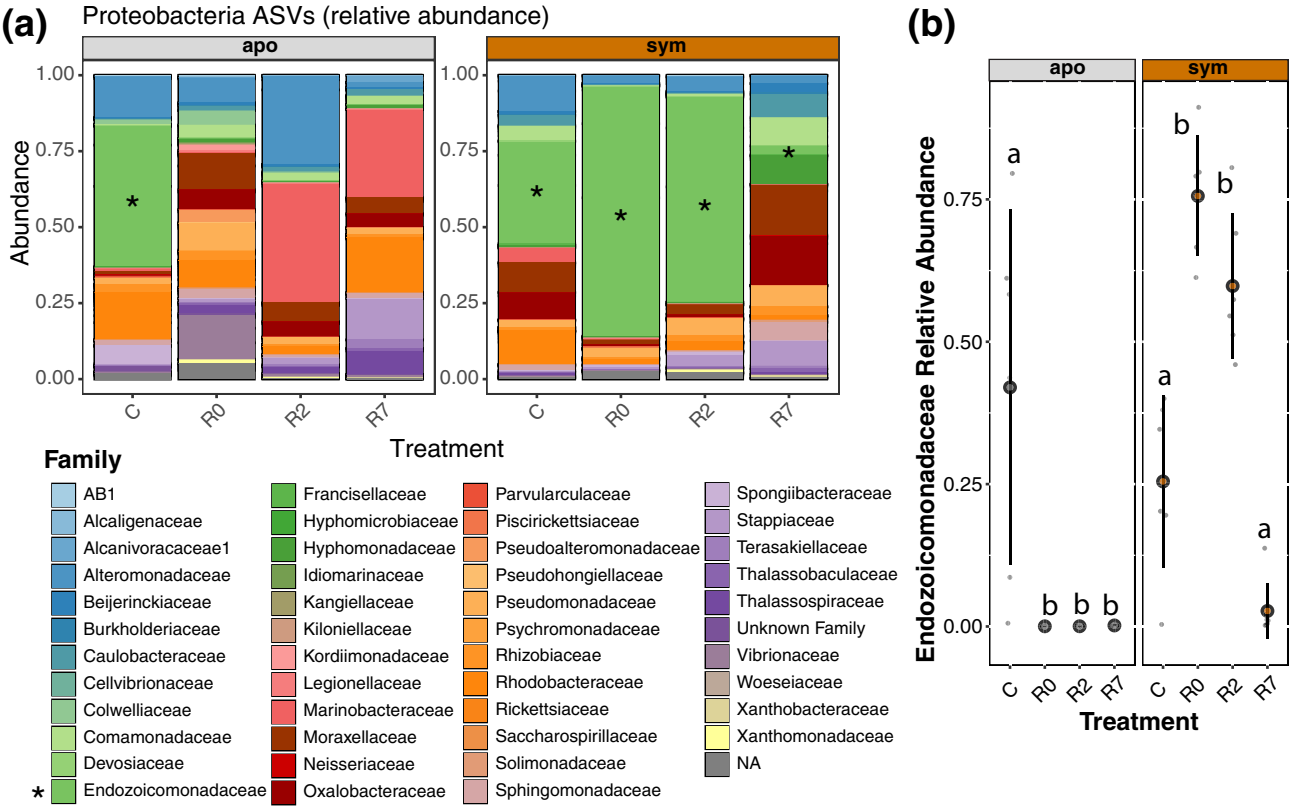

Fig. 3. Relative abundances of bacterial Families are impacted by antibiotic treatment and recovery. (**a**) Relative abundances of 16S ASVs within the Phylum Proteobacteria was measured across antibiotic treatments and symbiotic state (apo = aposymbiotic; sym = symbiotic). Colors in the stacked bar graph correspond to different bacterial Families. * denotes Endozoicomonadaceae in the legend and in the bar graphs (absent from aposymbiotic R0, R2, and R7 because the relative abundance is < 1%). (**b**) Relative abundances of the four ASVs in the Family Endozoicomonadaceae compared to all 264 ASVs were compared across antibiotic treatments and symbiotic states. Colored circles (gray, apo; orange, sym) show the mean, and black bars indicate standard deviation. Within each symbiotic state, distinct letters represent significant differences in Endozoicomonadaceae relative abundance across treatments (ANOVA and Tukey's post-hoc tests ($p < 0.01$)).

To identify DEGs between the control and antibiotic treatments in each symbiotic state, we performed pairwise comparisons of gene expression. In symbiotic Aiptasia, there were 1,000 DEGs between R0 and control samples, 983 DEGs between R2 and control samples, and 1,347 DEGs between R7 and control samples (FDR p-value < 0.05). In aposymbiotic Aiptasia, there were 342 DEGs between R0 and control samples, 958 DEGs between R2 and control samples, and 814 DEGs between R7 and control samples (FDR p-value < 0.05). We additionally determined the number of DEGs for all other possible pairwise comparisons within and between symbiotic states (Table S5).

To identify functional responses associated with microbiome depletion and recovery across symbiotic states, we performed GO enrichment analysis on BP terms between each antibiotic treatment and the control within each symbiotic state. This analysis showed that symbiotic and aposymbiotic R0 and R2 samples were positively enriched for functions relating to metabolism (e.g., "cellular lipid metabolic process;" "cofactor metabolic process;" "monosaccharide metabolic process) (FDR p-value < 0.1; Table S6). For both symbiotic states, 14 terms related to immune function (e.g., "regulation of interleukin-2 production;" "immune response") were decreased in R2 compared to controls, indicating that two days following antibiotic treatment, pathways related to immunity decreased in Aiptasia regardless of symbiotic state (Fig. 5b).

We also used WGCNAs to investigate the correlation between gene expression and experimental treatments/holobiont traits following antibiotic treatment and recovery. In the combined symbiotic and aposymbiotic WGCNA, 16,345 genes were assigned to 10 modules (Fig. S4). The Blue module (containing 4,348 genes) was enriched for GO terms related to immunity (Table S1). This module was positively correlated with aposymbiotic anemones, control, R0, and R7 treatments in aposymbiotic Aiptasia, as well as normalized CFU counts (Fig. S4). This module was negatively correlated with symbiotic anemones, the R2 treatment overall, the R2 treatment in symbiotic Aiptasia, and Endozoicomonadaceae relative abundances (Fig. S4).

Because symbiotic state influenced overall gene expression patterns, transcriptomic signals specific to antibiotic treatment may be masked in the combined WGCNA approach. To account for this issue, we performed separate WGCNAs on symbiotic and aposymbiotic samples. In the aposymbiotic-only WGCNA, 16,920 genes were assigned to 13 modules (Fig. S5). The Blue module (containing 3,429 genes) was enriched

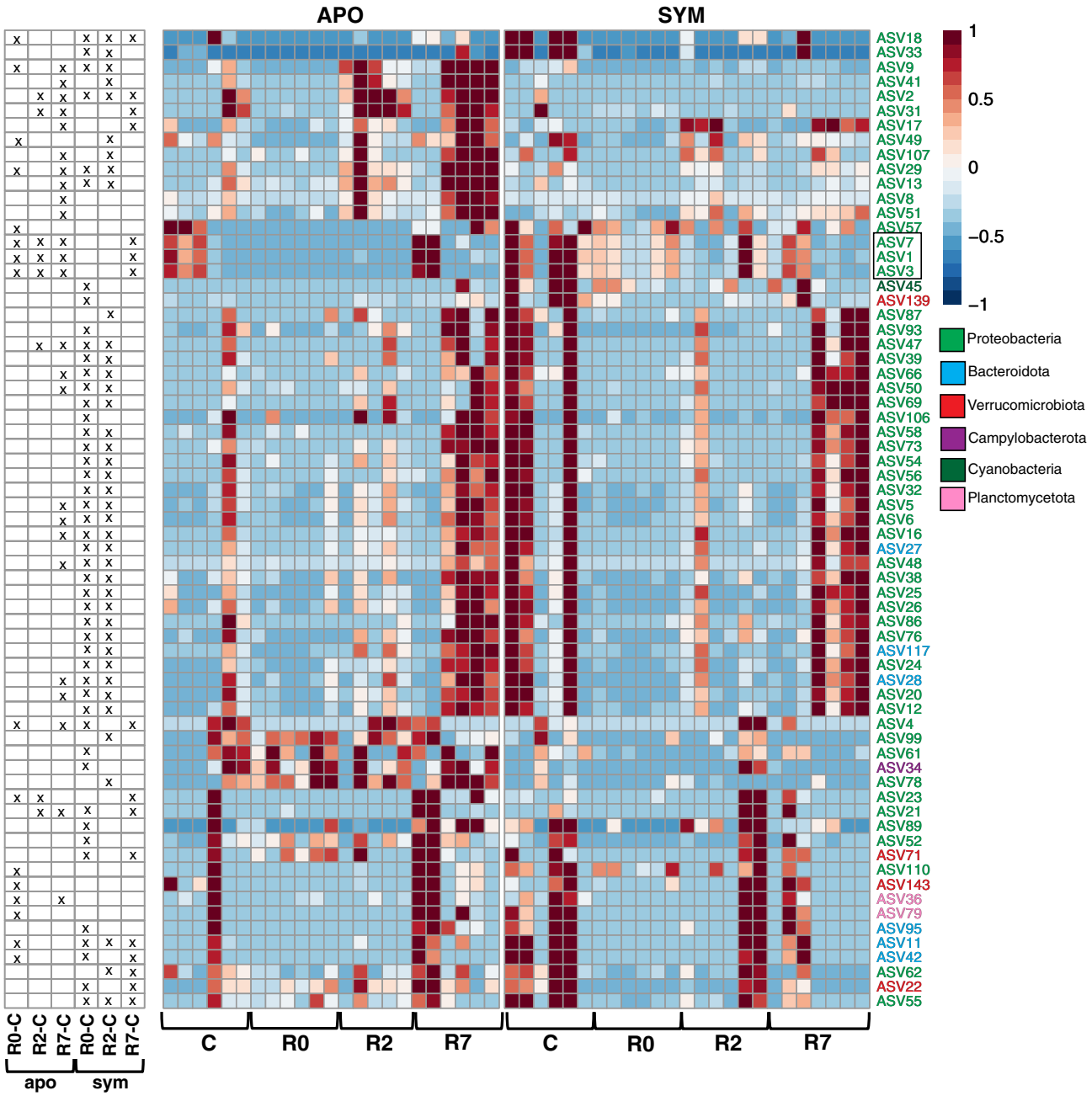

Fig. 4. Similar bacterial communities reestablish in symbiotic, but not aposymbiotic, Aiptasia following antibiotic treatment. Heatmap of ASVs with differential abundance in the indicated treatment conditions relative to controls within each symbiotic state. The color scale represents $\log_2$-transformed abundance of each ASV (row) in each anemone (column) relative to the mean ASV abundance across all anemones in that symbiotic state. ASVs are hierarchically clustered (dendrogram not shown) based on similar abundance across samples and are colored by their Phylum. A box is drawn around ASVs in the Family Endozoicomonadaceae. In the left panel, **x** indicates which ASVs have significantly different abundances in each treatment compared to the respective control (FDR p-value < 0.05).

for GO terms related to immunity. While terms relating explicitly to the NF-κB pathway were not identified, the term "Response to Tumor Necrosis Factor" was identified (Table S2). This module positively correlated with control anemones, CFU counts, and Endozoicomonadaceae relative abundance (Fig. S5). 565 Blue module genes annotated with immune GO terms were identified, 15 of which were differentially expressed in aposymbiotic R0 anemones compared to aposymbiotic controls. 17 immune genes in the Blue module were differentially expressed in aposymbiotic R2 anemones compared to aposymbiotic controls, and 9 Blue module genes were differentially expressed in the aposymbiotic R7 anemones compared to the aposymbiotic controls (Fig. 5c).

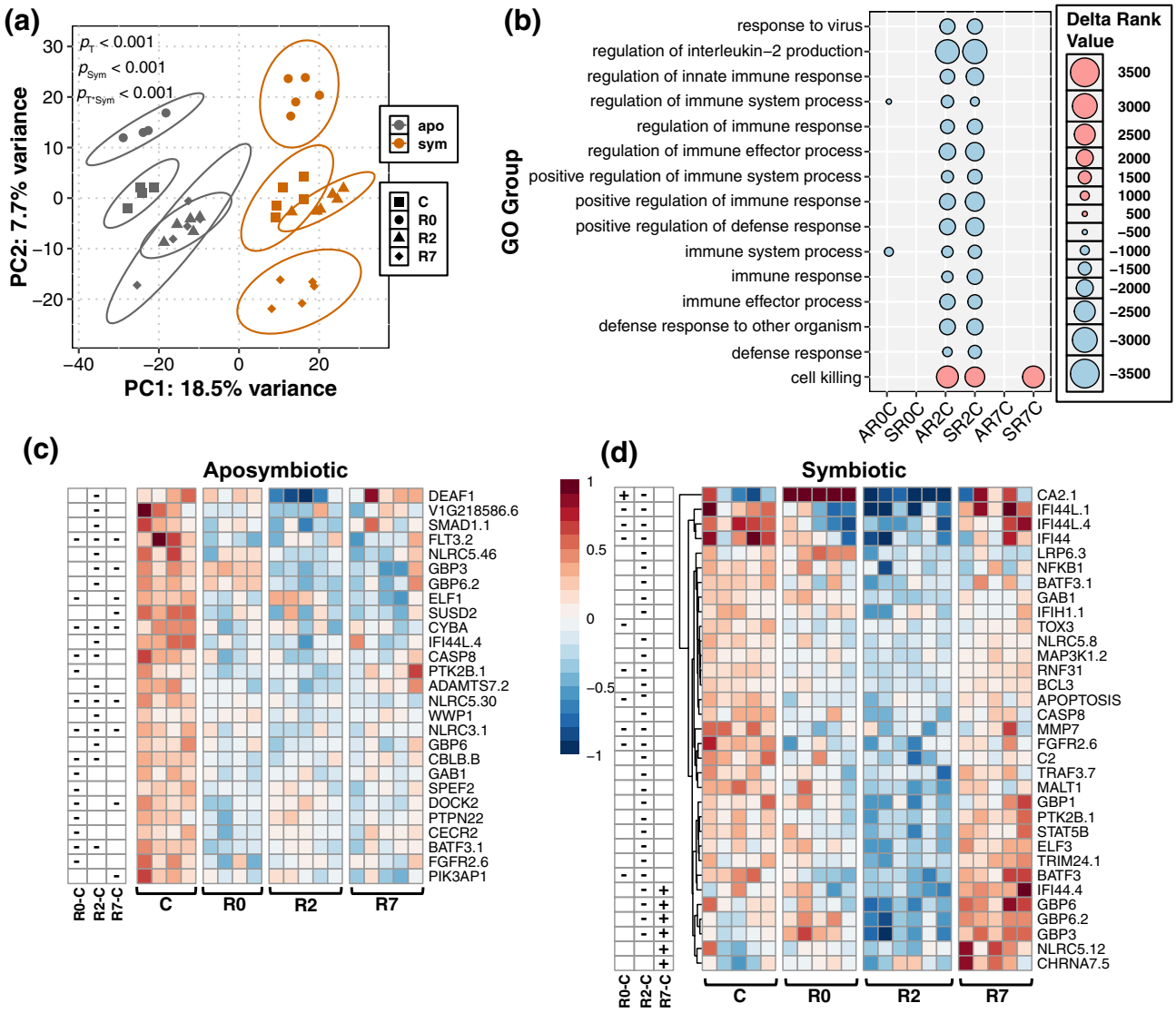

Fig. 5. Microbiome depletion and reestablishment modify host immune gene expression in symbiotic and aposymbiotic Aiptasia. (**a**) Principal component analysis (PCA) of $\log_2$-transformed counts for aposymbiotic (gray) and symbiotic (orange) Aiptasia across antibiotic treatments (shapes). PERMANOVA results for the effect of antibiotic treatment (p_T), symbiotic state (p_{Sym}) and their interaction (p_{T*Sym}) are included. (**b**) Delta rank values (represented by point size) of enriched Gene Ontology (GO) terms related to immunity were compared across each treatment relative to controls. Terms were plotted if they were significantly enriched in the treatment (red, positive Delta Rank Values) or enriched in the control (blue, negative Delta Rank Values) in at least two comparisons. AR0C = aposymbiotic R0 to aposymbiotic control; SR0C = symbiotic R0 to symbiotic control; AR2C = aposymbiotic R2 to aposymbiotic control. SR2C = symbiotic R2 to symbiotic control; AR7C = aposymbiotic R7 to aposymbiotic control; SR7C = symbiotic R7 to symbiotic control. (**c**) In aposymbiotic Aiptasia, genes were identified within the Blue WGCNA module that were annotated with enriched immune GO terms and found to be differentially expressed between R0 and control, R2 and control, or R7 and control. (**d**) In symbiotic Aiptasia, genes were identified within the Black WGCNA module that were annotated with enriched immune GO terms and found to be differentially expressed between R0 and control, R2 and control, or R7 and control. In (**c**) and (**d**), the left panels indicate which genes are differentially expressed (+ represents positive differential expression in the treatment compared to controls; - represents negative differential expression in the treatment compared to controls; FDR p-value < 0.05).

In the symbiotic-only WGCNA, 16,283 genes were assigned to 16 modules (Fig. S6). The Black module (containing 1,659 genes) was enriched for GO terms related to immunity, including the NF-κB pathway (Table S3). This module was positively correlated with the R7 treatment and negatively correlated with the R2 treatment, Endozoicomonadaceae abundance, and R-value change (Fig. S6). 941 Black module genes were annotated with immune GO terms, 10 of which were differentially expressed in symbiotic R0 compared to symbiotic controls. 30 immune genes in the Black module were differentially expressed in symbiotic R2 compared to symbiotic

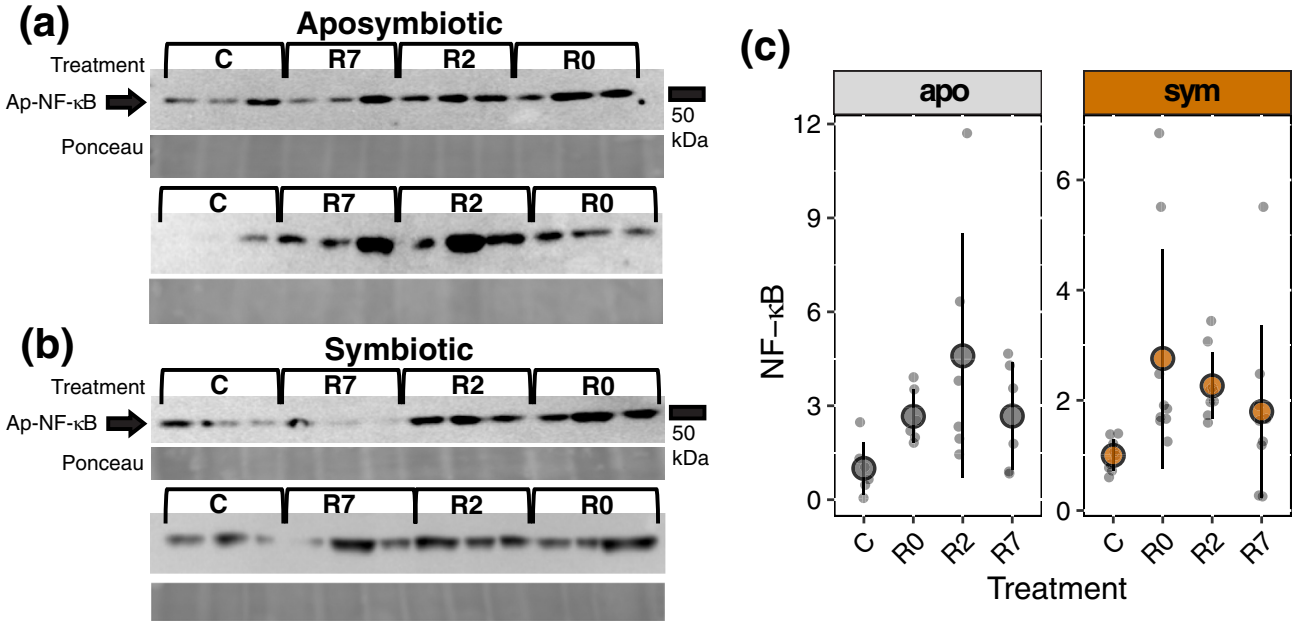

Fig. 6. Higher NF-κB protein levels in symbiotic and aposymbiotic Aiptasia following microbiome depletion. Western blots of NF-κB in aposymbiotic (**a**) and symbiotic (**b**) Aiptasia across antibiotic conditions. Two representative blots for each symbiotic state are shown. Three independent anemones were analyzed for each treatment in each Western blot. NF-κB levels were normalized to Ponceau staining for each sample. Location of the 50 kDa molecular weight marker is indicated to the right of the blots. (**c**) Levels of the processed form of NF-κB were normalized to total protein (Ponceau) for each anemone, and this value was normalized to the average control NF-κB:Ponceau value for each respective blot, then plotted. Colored circles (gray, apo; orange, sym) show the mean and black bars indicate standard deviation. Full-length blots and the corresponding Ponceau stains of the membranes are included in the Supplementary Material (Fig. S1a-j).

controls, and 6 immune genes in the Black module were differentially expressed in symbiotic R7 compared to symbiotic controls (Fig. 5d).

Symbiotic Aiptasia had a stronger transcriptomic response than aposymbiotic Aiptasia, including in expression of immune genes. However, in both symbiotic states, immune system pathways were differentially affected during microbiome reestablishment. Immune pathway genes downregulated in R2 anemones included genes involved in the NF-κB pathway (e.g., *NFKB1, BCL3, IFI44.4*, and *ELF3* in symbiotic Aiptasia)[45,76], as well as other immune pathway genes downregulated throughout the course of recovery. Other potential immune system pathways involved in microbiome reestablishment in both symbiotic states included C-Type Lectin Receptor signaling (*MALT1, BCL3*), Tumor Necrosis Factor signaling (*TRAF3.7, BCL3, CYBA, CASP8, PTK2B.1, ADAMTS7.2*), NOD-Like Receptor signaling (*TRAF3.7, RNF31*), and the MAPK pathway (*MAP3K1.2, FGFR2.6*)[77]. Many of these immune pathway genes were no longer downregulated following seven days of recovery (R7), especially in symbiotic Aiptasia (Fig. 5c, d).

Protein levels of the active form of NF-κB increase in microbially-depleted Aiptasia

Because gene expression pathways related to immunity were decreased following microbiome depletion in Aiptasia, we tested the effect of antibiotic treatment on protein levels of NF-κB—a transcription factor associated with immunity and algal symbiosis in many organisms. In both symbiotic and aposymbiotic Aiptasia, levels of the processed (active) form of the NF-κB protein were higher in R0, R2, and R7 samples compared to levels in control anemones (Fig. 6a, b). In aposymbiotic Aiptasia, processed NF-κB levels were ~ 2.7 times higher in R0 samples compared to controls, ~ 4.6 times higher in R2 samples compared to controls, and ~ 2.7 times higher in R7 samples compared to controls (Fig. 6a). In symbiotic Aiptasia, processed NF-κB levels were ~ 2.3 times higher in R0 samples compared to controls, ~ 2.3 times higher in R2 samples compared to controls, and ~ 1.8 times higher in R7 samples compared to controls (Fig. 6b, c). Therefore, antibiotic treatment resulted in increased levels of processed NF-κB regardless of symbiotic state ($p < 0.05$; Fig. 6c), indicating that, while general immunity gene expression is downregulated following antibiotic treatment, levels of transcription factor NF-κB are increased. Blots of the full-length gels are included in the Supplementary Material (Fig. S1a-j).

Discussion

We investigated the tripartite interactions among cnidarians, their intracellular photosynthetic algae, and their microbiomes using the facultatively symbiotic sea anemone Aiptasia to determine how a cnidarian holobiont responds to environmental stress. Using an antibiotic cocktail, we depleted the microbiomes of symbiotic and aposymbiotic Aiptasia and investigated how these microbiomes reestablished using 16S sequencing and gene

expression profiling of the anemone host. Shifts in alpha and beta diversity indicated that aposymbiotic Aiptasia microbiomes became more disrupted immediately following antibiotic treatment, whereas the microbiomes of symbiotic Aiptasia remained more stable. Taxa in the Family Endozoicomonadaceae, a putatively beneficial bacteria to certain marine invertebrate holobionts[13–15], were depleted in aposymbiotic, but not symbiotic, Aiptasia under antibiotic treatment. Additionally, symbiotic Aiptasia had more resilient microbiome communities following one week of recovery from antibiotic treatment. For both symbiotic and aposymbiotic Aiptasia, antibiotic treatment (and presumably microbiome depletion) led to downregulation of host immune pathways, but increased levels of transcription factor NF-κB, suggesting that NF-κB is involved in a non-immune aspect of microbiome depletion or antibiotic treatment (e.g., a stress response). These results imply that symbiotic and aposymbiotic Aiptasia have different capacities for microbiome stability following dysbiosis, but that they employ similar molecular mechanisms during microbiome reestablishment.

In agreement with previous work[21], we observed transient changes in algal symbiont density in symbiotic Aiptasia following antibiotic treatment. Here, R2 anemones lost color; however, after one week of recovery (R7), anemones recovered pigmentation associated with algal symbionts. These results indicate that some gene expression and immune protein responses in R2 anemones could be due to changes in symbiont density. However, previous studies in Aiptasia have demonstrated that active NF-κB protein levels do not significantly increase until approximately 99% of symbionts have been lost[44]. While we used different methods of symbiont density assessment, R2 anemones were still visually pigmented, indicating that a high level of symbiont loss did not occur, and, therefore, increased levels of active NF-κB were not due to symbiont loss. Other metrics of host physiological responses to antibiotic treatment[19] were not measured here, but may be important to consider in future studies.

We found that antibiotic treatment significantly impacted beta diversity (here defined as dissimilarity) in both symbiotic and aposymbiotic Aiptasia. Recovery from antibiotic treatment constrained community diversity in symbiotic Aiptasia, suggesting that symbiotic anemones can regulate and stabilize their remaining microbiome following antibiotic treatment. In contrast, this trend was not observed in aposymbiotic Aiptasia. Higher beta diversity indicates higher microbiome variability across samples within a treatment. In cnidarians, various environmental stressors have been shown to increase microbiome beta diversity[78]. As posited by the Anna Karenina principle, stochastic microbiome changes are associated with instability[79], which may lead to dysbiosis[29]. Conversely, microbiome stability has been linked to increased resilience to heat-induced bleaching[28,30]. In Aiptasia, increased microbiome stability observed in symbiotic anemones during recovery may indicate higher resilience to environmental stress.

Alpha diversity metrics describe microbiome diversity of individual samples. We found that three of the four measured metrics of alpha diversity differed in symbiotic versus aposymbiotic Aiptasia across antibiotic treatments. In symbiotic Aiptasia, inverse Simpson's Index, Shannon Index, and Evenness decreased before returning to baseline levels, whereas in aposymbiotic Aiptasia, these metrics increased before returning to baseline levels. Interestingly, previous research has demonstrated that environmental stressors (e.g., decreased pH, hypersalinity, and pollution) increase metrics of alpha diversity[80–83]. Our demonstration that Richness decreased following antibiotic exposure in both symbiotic and aposymbiotic Aiptasia corroborates previous work on microbiome depletion in anemones[21]. Together, we hypothesize that the increased susceptibility of aposymbiotic Aiptasia to microbiome depletion indicates that they are in a stressed holobiont state.

In contrast to previous studies that failed to identify *Endozoicomonas* ASVs in Aiptasia[20,25], we observed a high relative abundance of Endozoicomonadaceae in control anemones of both symbiotic states. Notably, the previous studies that did not identify Aiptasia-associated *Endozoicomonas* used CC7 Aiptasia hosting a non-native symbiont *Breviolum minutum*[20,25], whereas our symbiotic CC7 Aiptasia hosted the native symbiont *Symbiodinium linucheae*. While different Symbiodiniaceae strains share a core microbiome of Alphaproteobacteria and Gammaproteobacteria ASVs, they also harbor distinct ASVs by strain[6], yielding potentially different benefits to their native hosts and serving as potential reservoirs for microbiome repopulation following a disturbance. Indeed, *Pocillopora acuta* hosting *Cladocopium* algal symbionts have higher relative abundances of *Endozoicomonas* in their microbiomes compared to *P. acuta* hosting *Durusdinium* algal symbionts[84], supporting the idea that different algae can play a role in microbiome dynamics. Another striking observation from our data was the sustained depletion of Endozoicomonadaceae ASVs and their overall relative abundance in aposymbiotic compared to symbiotic Aiptasia. *Endozoicomonas* has been consistently identified as an important beneficial microbe to reef-building coral and other marine invertebrates (e.g., sponges)[13–15], and depletion in *Endozoicomonas* relative abundance is a common feature following exposure to environmental stress in multiple stony coral species[29]. *Endozoicomonas* has recently drawn attention for its proposed interaction with algal symbionts within coral hosts. In multiple coral species, including *Acropora loripes*[85] and *Stylophora pistillata*[86], host-specific strains of *Endozoicomonas* have been shown to form coral-associated microbial aggregates (CAMAs) within host tissues. In *A. loripes*, certain *Endozoicomonas* CAMAs tightly co-localized with algal symbionts[85]. Additionally, different *Endozoicomonas* clades may have different effects on sugar, lipid, and phosphorous metabolism[16]. The association between *Endozoicomonas* and Symbiodiniaceae, and the putative clade-specific roles of different *Endozoicomonas* in nutrient cycling, is consistent with there being metabolic interactions between these two symbionts within certain cnidarian hosts. Here, Endozoicomonadaceae depletion in aposymbiotic Aiptasia compared to the transient relative increase of its relative abundance in symbiotic Aiptasia is consistent with this proposed association. More specifically, our observations suggest that, because algal symbionts are housed within the symbiosome, an interaction between Symbiodiniaceae and Endozoicomonadaceae may buffer these bacteria from antibiotic-induced expulsion.

Beyond Endozoicomonadaceae, symbiotic antibiotic-treated Aiptasia recovered similar bacterial communities to controls, indicating that symbiotic Aiptasia may employ similar strategies to microbiome regulators by maintaining stable microbiomes and relying on gene expression or physiological plasticity to

withstand environmental challenges[31]. Conversely, aposymbiotic Aiptasia failed to reestablish similar bacterial communities to untreated Aiptasia after seven days, suggesting that these anemones are more analogous to microbiome conformers, which alter their microbiomes in order to survive adverse conditions[31]. While these terms (regulators and conformers) have been traditionally used for different host species, it is possible that, within a single species, individuals in different symbiotic states employ these same strategies.

In aposymbiotic anemones, we also observed increases in the relative abundances of the Families Marinobacteraceae and Moraxellaceae following antibiotic treatment. ASVs in both of these families have been associated with healthy cnidarians and holobiont tolerance to environmental stress[87–90]. In aposymbiotic Aiptasia, increases in Marinobacteraceae and Moraxellaceae coupled with the loss of Endozoicomonadaceae may thus represent a shift from one healthy microbiome to another healthy microbiome following antibiotic treatment and recovery, rather than colonization by opportunistic and pathogenic bacteria. For example, some Moraxellaceae members may aid in host carbon recycling[91], and Marinobacteraceae members may contribute to thermotolerance under certain conditions in Aiptasia[89]. However, other studies have observed rapid and prominent increases in the relative abundance of Moraxellaceae following environmental change, suggesting that Moraxellaceae is an indicator of holobiont stress[36,37], consistent with our observations in aposymbiotic Aiptasia. Additional work on these less-studied taxa is warranted.

Our gene expression results provide insight into the processes by which Aiptasia reestablishes bacterial communities following depletion. While both symbiotic states showed altered gene expression profiles following antibiotic treatment and recovery, symbiotic Aiptasia exhibited greater transcriptomic shifts, signified by higher numbers of DEGs in each treatment compared to the controls relative to aposymbiotic Aiptasia. Higher transcriptomic plasticity[92] further supports that symbiotic Aiptasia are akin to microbiome regulators in that, during environmental stress, rather than altering their microbiome, they differentially regulate gene expression pathways[31]. Transcriptomic plasticity in combination with microbiome stability has been proposed in a stony coral, as well[93]. Interestingly, other studies have revealed that symbiotic state often influences phenotypic responses (transcriptomic, physiological, etc.) to environmental stressors[32,45,94]. For example, our study in Aiptasia is consistent with previous research on cold stress responses in the facultatively symbiotic coral *Astrangia poculata*[95], wherein symbiotic hosts exhibited stronger transcriptomic responses than aposymbiotic hosts[95]. In contrast, under starvation stress, aposymbiotic Aiptasia had stronger transcriptomic responses than symbiotic Aiptasia[45]. In a study on thermal stress in the facultatively symbiotic coral *Oculina arbuscula*, no differences in the magnitude of responses across symbiotic states were observed[96]. These results indicate that symbiotic state differentially modulates host responses depending on the species and the stressor.

While the strength of the transcriptomic response to antibiotic treatment differed by symbiotic state, symbiotic and aposymbiotic Aiptasia both showed similar patterns in specific pathways following microbiome depletion and recovery. Of note, processes relating to host metabolism were enriched following microbiome depletion, suggesting that bacterial taxa involved in nutrient cycling were depleted[29,97], and that hosts compensate for this energetic loss by increasing metabolism. In contrast, gene expression profiles of both symbiotic and aposymbiotic Aiptasia showed downregulation of immune system pathways early in recovery from antibiotic treatment, presumably to allow for reestablishment of depleted bacteria. Notably, C-Type Lectin Receptor signaling, Tumor Necrosis Factor signaling, NOD-Like Receptor signaling, the MAPK pathway, and the NF-κB pathway may be implicated in selective reestablishment of the microbiome. However, it is also possible that this downregulation of immune pathways is due to reductions in bacterial load more broadly, whose presence may elicit a stress response given that they are foreign organisms invading a host. In contrast, "cell killing" gene pathways were positively enriched following antibiotic treatment, which may have contributed to loss of both bacterial and algal symbionts.

Although some immune gene expression pathways were downregulated following microbiome depletion in symbiotic and aposymbiotic Aiptasia, active NF-κB protein levels increased following microbiome depletion. The Ap-NF-κB protein is regulated post-translationally (i.e., truncation of the C-terminal inhibitory domain)[44]. Thus, gene expression and NF-κB protein activity levels may not necessarily correlate.

Recent work highlights the importance of immune system pathways for selective uptake of compatible algal symbionts in Aiptasia[77], indicating potentially shared pathways by which the host regulates microbial and algal symbionts. Nevertheless, our results do not clearly separate the effects of algal symbiont loss and microbiome loss on host gene expression. Most studies exploring interactions between host immunity and the microbiome have focused on how the microbiome influences disease susceptibility[35,98,99]. However, research in other systems, including human disease models, has revealed a great deal about the molecular interactions between the microbiome and the host immune system. For example, in mammals, the host immune system can selectively distinguish between microbiome-associated and pathogenic bacteria[100]. Additionally, a wide breadth of research has investigated immunosuppression following antibiotic usage in human disease models[101], highlighting the importance of a stable microbiome for proper immune system function. Based on our results, we propose that, following microbiome dysbiosis, the Aiptasia host immune system is downregulated to allow for microbiome reestablishment, which may be an evolutionarily conserved mechanism for microbiome regulation across metazoans. Further investigation into the consequences of downregulated gene expression pathways on organismal immunity to pathogen challenge is warranted. Additionally, parsing out the effect of bacterial and algal symbionts on host immunity by using axenic algal strains and microbially depleted hosts is a future avenue worth exploration[20,102,103]. This research also has implications for conservation biology, as researchers rapidly respond to coral disease with antibiotic[104] and probiotic[105] treatments. For example, it highlights that Endozoicomonadaceae can associate with algal symbionts to potentially increase holobiont resilience under environmental change.

Data availability

Raw fastq files for all metabarcoding and gene expression samples are publicly available on the Sequence Read Archive BioProject PRJNA1336731. All data and code can be found here: [https://github.com/mariaingersoll/Aiptasia_Microbiome.git] (https:/github.com/mariaingersoll/Aiptasia_Microbiome.git).

Received: 9 December 2025; Accepted: 30 January 2026
Published online: 25 February 2026

References

1. Maire, J. et al. Effects of ocean warming on the underexplored members of the coral microbiome. *Integr. Comp. Biol.* **62**, 1700–1709 (2022).
2. McCauley, M., Goulet, T. L., Jackson, C. R. & Loesgen, S. Systematic review of cnidarian microbiomes reveals insights into the structure, specificity, and fidelity of marine associations. *Nat. Commun.* **14**, 4899 (2023).
3. Pollock, F. J. et al. Coral-associated bacteria demonstrate phylosymbiosis and cophylogeny. *Nat. Commun.* **9**, 4921 (2018).
4. Ainsworth, D. T. et al. The coral core microbiome identifies rare bacterial taxa as ubiquitous endosymbionts. *ISME J.* **9**, 2261–2274 (2015).
5. Frommlet, J. C. et al. Coral symbiotic algae calcify ex hospite in partnership with bacteria. *Proc. Natl. Acad. Sci. USA* **112**, 6158–6163 (2015).
6. Lawson, C. A., Raina, J.-B., Kahlke, T., Seymour, J. R. & Suggett, D. J. Defining the core microbiome of the symbiotic dinoflagellate. *Symbiodinium. Environ. Microbiol. Rep.* **10**, 7–11 (2018).
7. Maire, J. et al. Intracellular bacteria are common and taxonomically diverse in cultured and in hospite algal endosymbionts of coral reefs. *ISME J.* **15**, 2028–2042 (2021).
8. Reshef, L., Koren, O., Loya, Y., Zilber-Rosenberg, I. & Rosenberg, E. The coral probiotic hypothesis. *Environ. Microbiol.* **8**, 2068–2073 (2006).
9. Ritchie, K. B. Regulation of microbial populations by coral surface mucus and mucus-associated bacteria. *Mar. Ecol. Prog. Ser.* **322**, 1–14 (2006).
10. Delgadillo-Ordoñez, N. et al. Probiotics reshape the coral microbiome in situ without detectable off-target effects in the surrounding environment. *Commun. Biol.* **7**, 1–16 (2024).
11. Peixoto, R. S., Rosado, P. M., de Leite, D. C. A., Rosado, A. S. & Bourne, D. G. Beneficial Microorganisms for Corals (BMC): Proposed mechanisms for coral health and resilience. *Front. Microbiol.* **8**, 341 (2017).
12. Pogoreutz, C. & Ziegler, M. Frenemies on the reef? Resolving the coral–*Endozoicomonas* association. *Trends Microbiol.* **32**, 422–434 (2024).
13. Tandon, K. et al. Comparative genomics: Dominant coral-bacterium Endozoicomonas acroporae metabolizes dimethylsulfoniopropionate (DMSP). *ISME J.* **14**, 1290–1303 (2020).
14. Neave, M. J., Michell, C. T., Apprill, A. & Voolstra, C. R. Endozoicomonas genomes reveal functional adaptation and plasticity in bacterial strains symbiotically associated with diverse marine hosts. *Sci. Rep.* **7**, 40579 (2017).
15. Rua, C. P. J. et al. Diversity and antimicrobial potential of culturable heterotrophic bacteria associated with the endemic marine sponge *Arenosclera brasiliensis*. *PeerJ* **2**, e419 (2014).
16. Gotze, C. R. et al. Genomic prediction of symbiotic interactions between two Endozoicomonas clades and their coral host. *Acropora loripes. Anim. Microbiome* **7**, 94 (2025).
17. Hoegh-Guldberg, O. Coral reef ecosystems and anthropogenic climate change. *Reg. Environ. Chang.* **11**, 215–227 (2011).
18. Jacobovitz, M. R., Hambleton, E. A. & Guse, A. Unlocking the complex cell biology of coral–dinoflagellate symbiosis: A model systems approach. *Annu. Rev. Genet.* **57**, 411–434 (2023).
19. Bent, S. M., Miller, C. A., Sharp, K. H., Hansel, C. M. & Apprill, A. Differential patterns of microbiota recovery in symbiotic and aposymbiotic corals following antibiotic disturbance. *mSystems* **6**, e01086-e1120 (2021).
20. Costa, R. M. et al. Surface topography, bacterial carrying capacity, and the prospect of microbiome manipulation in the sea anemone coral model Aiptasia. *Front. Microbiol.* **12**, 637834 (2021).
21. MacVittie, S., Doroodian, S., Alberto, A. & Sogin, M. Microbiome depletion and recovery in the sea anemone, Exaiptasia diaphana, following antibiotic exposure. *mSystems* **9**, e01342-23 (2024).
22. Bove, C. B. et al. Exposure to global change and microplastics elicits an immune response in an endangered coral. *Front. Mar. Sci.* **9**, 1037130 (2023).
23. Chan, W. Y., Peplow, L. M., Menéndez, P., Hoffmann, A. A. & van Oppen, M. J. H. The roles of age, parentage and environment on bacterial and algal endosymbiont communities in Acropora corals. *Mol. Ecol.* **28**, 3830–3843 (2019).
24. Curtis, E., Moseley, J., Racicot, R. & Wright, R. M. Bacterial microbiome variation across symbiotic states and clonal lines in a cnidarian model. *Front. Mar. Sci.* **10**, 1113043 (2023).
25. Röthig, T. et al. Distinct bacterial communities associated with the coral model aiptasia in aposymbiotic and symbiotic states with symbiodinium. *Front. Mar. Sci.* **3**, 234 (2016).
26. Grupstra, C. G. B. et al. Holobiont traits shape climate change responses in cryptic coral lineages. *Glob. Chang. Biol.* **30**, e17578 (2024).
27. Savary, R. et al. Fast and pervasive transcriptomic resilience and acclimation of extremely heat-tolerant coral holobionts from the northern Red Sea. *Proc. Natl. Acad. Sci. USA* **118**, e2023298118 (2021).
28. Ziegler, M., Seneca, F. O., Yum, L. K., Palumbi, S. R. & Voolstra, C. R. Bacterial community dynamics are linked to patterns of coral heat tolerance. *Nat. Commun.* **8**, 14213 (2017).
29. McDevitt-Irwin, J. M., Baum, J. K., Garren, M. & Vega Thurber, R. L. Responses of coral-associated bacterial communities to local and global stressors. *Front. Mar. Sci.* **4**, 262 (2017).
30. Grottoli, A. G. et al. Coral physiology and microbiome dynamics under combined warming and ocean acidification. *PLoS ONE* **13**, e0191156 (2018).
31. Ziegler, M. et al. Coral bacterial community structure responds to environmental change in a host-specific manner. *Nat. Commun.* **10**, 3092 (2019).
32. Da-Anoy, J. et al. Microbial depletion is associated with slower cnidarian regeneration. *Integr. Comp. Biol.* **65**, 139–151 (2025).
33. van de Water, J. A. J. M. et al. The coral immune response facilitates protection against microbes during tissue regeneration. *Mol. Ecol.* **24**, 3390–3404 (2015).
34. Welsh, R. M. et al. Alien vs. predator: Bacterial challenge alters coral microbiomes unless controlled by Halobacteriovorax predators. *PeerJ* **5**, e3315 (2017).
35. Young, B. D. et al. Different disease inoculations cause common responses of the host immune system and prokaryotic component of the microbiome in *Acropora palmata*. *PLoS ONE* **18**, e0286293 (2023).
36. Hsieh, Y. E. et al. Successive responses of three coral holobiont components (coral hosts, symbiotic algae, and bacteria) to daily temperature fluctuations. *Ecol. Indic.* **158**, 111515 (2024).
37. Li, J., Long, L., Zou, Y. & Zhang, S. Microbial community and transcriptional responses to increased temperatures in coral *Pocillopora damicornis* holobiont. *Environ. Microbiol.* **23**, 826–843 (2021).

38. Han, Y. et al. Opportunistic bacteria with reduced genomes are effective competitors for organic nitrogen compounds in coastal dinoflagellate blooms. *Microbiome* **9**, 71 (2021).
39. Mayali, X., Weber, P. K., Mabery, S. & Pett-Ridge, J. Phylogenetic patterns in the microbial response to resource availability: Amino acid incorporation in San Francisco Bay. *PLoS ONE* **9**, e95842 (2014).
40. Frommlet, J., Guimarães, B., Sousa, L., Serôdio, J. & Alves, A. *Neptunomonas phycophila* sp. nov. isolated from a culture of *Symbiodinium* sp., a dinoflagellate symbiont of the sea anemone *Aiptasia tagetes*. *Int. J. Syst. Evol. Microbiol.* **65**, 915–919 (2015).
41. McCauley, M. et al. Manipulation of the Symbiodiniaceae microbiome confers multigenerational impacts on symbioses and reproductive ecology of its *Exaiptasia diaphana* host. *ISME J.* **19**, wraf189 (2025).
42. Miccoli, A., Picchietti, S., Fausto, A. M. & Scapigliati, G. Evolution of immune defence responses as incremental layers among Metazoa. *Eur. Zool. J.* **88**, 44–57 (2021).
43. Mansfield, K. M. & Gilmore, T. D. Innate immunity and cnidarian-Symbiodiniaceae mutualism. *Dev. Comp. Immunol.* **90**, 199–209 (2019).
44. Mansfield, K. M. et al. Transcription factor NF-κB is modulated by symbiotic status in a sea anemone model of cnidarian bleaching. *Sci. Rep.* **7**, 16025 (2017).
45. Valadez-Ingersoll, M. et al. Starvation differentially affects gene expression, immunity and pathogen susceptibility across symbiotic states in a model cnidarian. *Proc. R. Soc. B* **291**, 20231685 (2024).
46. Dani, V. et al. Thermal and menthol stress induce different cellular events during sea anemone bleaching. *Symbiosis* **69**, 175–192 (2016).
47. Ogle, D. H., Doll, J. C., Wheeler, A. P. & Dinno, A. FSA: Simple Fisheries Stock Assessment Methods R package. (2025).
48. Winters, G., Holzman, R., Blekhman, A., Beer, S. & Loya, Y. Photographic assessment of coral chlorophyll contents: Implications for ecophysiological studies and coral monitoring. *J. Exp. Mar. Biol. Ecol.* **380**, 25–35 (2009).
49. R Core Team. R: The R Project for Statistical Computing. https://www.r-project.org/ (2023).
50. Apprill, A., McNally, S., Parsons, R. & Weber, L. Minor revision to V4 region SSU rRNA 806R gene primer greatly increases detection of SAR11 bacterioplankton. *Aquat. Microb. Ecol.* **75**, 129–137 (2015).
51. Parada, A. E., Needham, D. M. & Fuhrman, J. A. Every base matters: Assessing small subunit rRNA primers for marine microbiomes with mock communities, time series and global field samples. *Environ. Microbiol.* **18**, 1403–1414 (2016).
52. Posit team. RStudio: Integrated Development Environment for R. Posit Software, PBC (2025).
53. Valadez-Ingersoll, M. et al. Cell type-specific immune regulation under symbiosis in a facultatively symbiotic coral. *ISME J.* **19**, wraf132 (2025).
54. Martin, M. Cutadapt removes adapter sequences from high-throughput sequencing reads. *EMBnet.journal* **17**, 10–12 (2011).
55. Callahan, B. J., Sankaran, K., Fukuyama, J. A., McMurdie, P. J. & Holmes, S. P. Bioconductor workflow for microbiome data analysis: From raw reads to community analyses. *F1000Res* **5**, 1492 (2016).
56. Quast, C. et al. The SILVA ribosomal RNA gene database project: Improved data processing and web-based tools. *Nucleic Acids Res.* **41**, D590–D596 (2013).
57. Davis, N. M., Proctor, D. M., Holmes, S. P., Relman, D. A. & Callahan, B. J. Simple statistical identification and removal of contaminant sequences in marker-gene and metagenomics data. *Microbiome* **6**, 226 (2018).
58. Matz, M. V. MCMC.OTU: Bayesian analysis of multivariate counts data in DNA Metabarcoding and Ecology (2016).
59. Martinez Arbizu, P. pairwiseAdonis: Pairwise multilevel comparison using adonis. (2017).
60. Oksanen, J. *et al.* vegan: Community Ecology Package. (2024).
61. McMurdie, P. J. & Holmes, S. phyloseq: An R package for reproducible interactive analysis and graphics of microbiome census data. *PLoS ONE* **8**, e61217 (2013).
62. Wickham, H., François, R., Henry, L., Müller, K. & Vaughan, D. dplyr: A grammar of data manipulation R package. (2023).
63. Love, M. I., Huber, W. & Anders, S. Moderated estimation of fold change and dispersion for RNA-seq data with DESeq2. *Genome Biol.* **15**, 550 (2014).
64. Kolde, R. pheatmap: Pretty heatmaps. R package. (2019).
65. Meyer, E., Aglyamova, G. V. & Matz, M. V. Profiling gene expression responses of coral larvae (*Acropora millepora*) to elevated temperature and settlement inducers using a novel RNA-Seq procedure. *Mol. Ecol.* **20**, 3599–3616 (2011).
66. Hannon, G. J. FASTX-Toolkit. (2010).
67. Baumgarten, S. et al. The genome of Aiptasia, a sea anemone model for coral symbiosis. *Proc. Natl. Acad. Sci. USA* **112**, 11893–11898 (2015).
68. González-Pech, R. A. et al. Comparison of 15 dinoflagellate genomes reveals extensive sequence and structural divergence in family Symbiodiniaceae and genus Symbiodinium. *BMC Biol.* **19**, 73 (2021).
69. Langmead, B. & Salzberg, S. L. Fast gapped-read alignment with Bowtie 2. *Nat. Methods* **9**, 357–359 (2012).
70. Kauffmann, A., Gentleman, R. & Huber, W. arrayQualityMetrics—a bioconductor package for quality assessment of microarray data. *Bioinformatics* **25**, 415–416 (2009).
71. Wright, R. M., Aglyamova, G. V., Meyer, E. & Matz, M. V. Gene expression associated with white syndromes in a reef building coral, *Acropora hyacinthus*. *BMC Genom.* **16**, 371 (2015).
72. Wickham, H. *Ggplot2: Elegant graphics for data analysis (3e)* (Springer, 2016).
73. Langfelder, P. & Horvath, S. WGCNA: An R package for weighted correlation network analysis. *BMC Bioinform.* **9**, 559 (2008).
74. Radice, V. Z., Martinez, A., Paytan, A., Potts, D. C. & Barshis, D. J. Complex dynamics of coral gene expression responses to low pH across species. *Mol. Ecol.* **33**, e17186 (2024).
75. Carrión, P. J. A. et al. Starvation decreases immunity and immune regulatory factor NF-κB in the starlet sea anemone *Nematostella vectensis*. *Commun. Biol.* **6**, 1–10 (2023).
76. Cleves, P. A., Krediet, C. J., Lehnert, E. M., Onishi, M. & Pringle, J. R. Insights into coral bleaching under heat stress from analysis of gene expression in a sea anemone model system. *Proc. Natl. Acad. Sci. USA* **117**, 28906–28917 (2020).
77. Jacobovitz, M. R. et al. Dinoflagellate symbionts escape vomocytosis by host cell immune suppression. *Nat. Microbiol.* **6**, 769–782 (2021).
78. Zaneveld, J. R. et al. Overfishing and nutrient pollution interact with temperature to disrupt coral reefs down to microbial scales. *Nat. Commun.* **7**, 11833 (2016).
79. Zaneveld, J. R., McMinds, R. & Vega Thurber, R. Stress and stability: Applying the Anna Karenina principle to animal microbiomes. *Nat. Microbiol.* **2**, 17121 (2017).
80. Bourne, D., Iida, Y., Uthicke, S. & Smith-Keune, C. Changes in coral-associated microbial communities during a bleaching event. *ISME J.* **2**, 350–363 (2008).
81. Meron, D. et al. The impact of reduced pH on the microbial community of the coral *Acropora eurystoma*. *ISME J.* **5**, 51–60 (2011).
82. Röthig, T., Ochsenkühn, M. A., Roik, A., van der Merwe, R. & Voolstra, C. R. Long-term salinity tolerance is accompanied by major restructuring of the coral bacterial microbiome. *Mol. Ecol.* **25**, 1308–1323 (2016).
83. Ziegler, M. et al. Coral microbial community dynamics in response to anthropogenic impacts near a major city in the central Red Sea. *Mar. Pollut. Bull.* **105**, 629–640 (2016).
84. Yang, Q. et al. Symbiotic Symbiodiniaceae mediate coral-associated bacterial communities along a natural thermal gradient. *Environ. Microb.* **20**, 72 (2025).
85. Gotze, C. R. et al. Differential aggregation patterns of Endozoicomonas within tissues of the coral *Acropora loripes*. *ISME J.* **19**, wraf059 (2025).

86. Wada, N. et al. High-resolution spatial and genomic characterization of coral-associated microbial aggregates in the coral *Stylophora pistillata*. *Sci. Adv.* **8**, eabo2431 (2022).
87. Cheng, K. et al. Integrated metagenomic and metaproteomic analyses reveal bacterial micro-ecological mechanisms in coral bleaching. *mSystems* **8**, 00505–23 (2023).
88. Kvennefors, E. C. E., Sampayo, E., Ridgway, T., Barnes, A. C. & Hoegh-Guldberg, O. Bacterial communities of two ubiquitous Great Barrier Reef corals reveals both site- and species-specificity of common bacterial associates. *PLoS ONE* **5**, e10401 (2010).
89. Randle, J. L., Cárdenas, A., Gegner, H. M., Ziegler, M. & Voolstra, C. R. Salinity-conveyed thermotolerance in the coral model Aiptasia is accompanied by distinct changes of the bacterial microbiome. *Front. Mar. Sci.* **7**, 573635 (2020).
90. Sunagawa, S. et al. Generation and analysis of transcriptomic resources for a model system on the rise: the sea anemone *Aiptasia pallida* and its dinoflagellate endosymbiont. *BMC Genom.* **10**, 258 (2009).
91. Al-Dahash, L. M. & Mahmoud, H. M. Harboring oil-degrading bacteria: A potential mechanism of adaptation and survival in corals inhabiting oil-contaminated reefs. *Mar. Pollut. Bull.* **72**, 364–374 (2013).
92. Rivera, H. E. et al. A framework for understanding gene expression plasticity and its influence on stress tolerance. *Mol. Ecol.* **30**, 1381–1397 (2021).
93. Rodriguez-Casariego, J. A. et al. Multi-omic characterization of mechanisms contributing to rapid phenotypic plasticity in the coral *Acropora cervicornis* under divergent environments. *Coral Reefs* **43**, 53–66 (2024).
94. Chei, E., Conti-Jerpe, I. E., Pons, L. & Baker, D. M. Changes within the coral symbiosis underpin seasonal trophic plasticity in reef corals. *ISME Commun.* **5**, ycae162 (2025).
95. Wuitchik, D. M. et al. Photosymbiosis reduces the environmental stress response under a heat challenge in a facultatively symbiotic coral. *Sci. Rep.* **14**, 15484 (2024).
96. Aichelman, H. E. et al. Symbiosis modulates gene expression of symbionts, but not coral hosts, under thermal challenge. *Mol. Ecol.* **33**, e17318 (2024).
97. Bourne, D. G., Morrow, K. M. & Webster, N. S. Insights into the coral microbiome: Underpinning the health and resilience of reef ecosystems. *Annu. Rev. Microbiol.* **70**, 317–340 (2016).
98. Pollock, F. J. et al. Reduced diversity and stability of coral-associated bacterial communities and suppressed immune function precedes disease onset in corals. *R. Soc. Open Sci.* **6**, 190355 (2019).
99. Voolstra, C. R. et al. The coral microbiome in sickness, in health and in a changing world. *Nat. Rev. Microbiol.* **22**, 460–475 (2024).
100. Bessman, N. J. & Sonnenberg, G. F. Emerging roles for antigen presentation in establishing host–microbiome symbiosis. *Immunol. Rev.* **272**, 139–150 (2016).
101. Ubeda, C. & Pamer, E. G. Antibiotics, microbiota, and immune defense. *Trends Immunol.* **33**, 459–466 (2012).
102. Bove, C. B., Ingersoll, M. V. & Davies, S. W. Help Me, Symbionts, you're my only hope: Approaches to accelerate our understanding of coral holobiont interactions. *Integr. Comp. Biol.* **62**, 1756–1769 (2022).
103. Xiang, T., Hambleton, E. A., DeNofrio, J. C., Pringle, J. R. & Grossman, A. R. Isolation of clonal axenic strains of the symbiotic dinoflagellate Symbiodinium and their growth and host specificity(1). *J. Phycol.* **49**, 447–458 (2013).
104. Studivan, M. S. et al. Stony coral tissue loss disease intervention with amoxicillin leads to a reversal of disease-modulated gene expression pathways. *Mol. Ecol.* **32**, 5394–5413 (2023).
105. Ushijima, B. et al. Chemical and genomic characterization of a potential probiotic treatment for stony coral tissue loss disease. *Commun. Biol.* **6**, 248 (2023).

Acknowledgements

We thank the Tufts University Core Facility and the University of Texas at Austin Genomic Sequencing and Analysis Facility. We also thank the Boston University Marine Program, Kian Thompson, and Justin Scace for access to aquarium facilities and artificial seawater. We thank the Boston University Shared Computing Cluster for computational support.

Author contributions

Conceptualization: M.V.-I., T.D.G., S.W.D.; Methodology: M.V.-I., C.A.B., E.X.F., A.W.; Analysis: M.V.-I., C.A.B., E.X.F, A.W.; Writing—Original Draft: M.V.-I, T.D.G., S.W.D.; Writing—Reviewing and Editing: M.V.-I., C.A.B., E.X.F., A.W., T.D.G., S.W.D.; Resources: T.D.G., S.W.D.; Funding: T.D.G., S.W.D.

Funding

This research was supported by a National Science Foundation grant IOS-1937650 (to T.D.G. and S.W.D.). M,V.-I. was supported by a National Science Foundation Graduate Research Fellowship, a National Science Foundation NRT DGE 1735087, and a Boston University Marine Program Warren McLeod Graduate Fellowship. C.A.B. was supported by an NSF Research Experiences for Undergraduates grant, and C.A.B. and A.W. were supported by the Boston University Undergraduate Research Opportunities Program.

Competing interests

The authors declare no competing interests.

Additional information

Supplementary Information The online version contains supplementary material available at https://doi.org/10.1038/s41598-026-38684-4.

Correspondence and requests for materials should be addressed to S.W.D.